13 Phase transitions and superconducting photon detectors

D. Destraz (Master student until June 2015), A. Engel (until January 2016), A. Gazizulina, F. von Rohr (until December 2015) , H. Grundmann, S. Huangfu (since October 2015), A. Schilling, S. Siegrist, Q. Wang (since November 2015) and Z. Xiaofu

in collaboration with:
University of Bern (K. Krämer), Forschungszentrum Karlsruhe (Th. Wolf, H. Küpfer), Karlsruhe Institut für Technologie (K. Ilín), Deutsches Zentrum für Luft- und Raumfahrt (H.-W. Hübers, A. Semenov), University of Wellington (B. Ruck), FIRST Lab ETH Zürich, PSI Villigen (K. Conder, V. Pomjakushin, M. Medarde), ETH Zürich (R. Nesper), LMU München (W. Schnick), Princeton University (R. J. Cava), HZ Berlin (D. Quintero-Castro, B. Lake, I. Glavatskyi)

13.1 X-ray sensitive superconducting photon detectors

As one of the most interesting early results in our project on X-ray sensitive superconducting nanowire single-photon detectors (SNSPD) we had observed an X-ray energy dependence of the detector pulse height histograms [1] (see also annual report 2011/12). A quantitative analysis of the X-SNSPD energy resolution was impossible since our X-ray tube produces a continuous energy spectrum. In a bachelor project [2] we have developed an X-ray fluorescence setup that produces quasi-monochromatic X-rays at the cost of a significant intensity loss. The new setup allows to vary the photon energy by a simple exchange the target material.

In another bachelor project [3] we have amended a numerical model simulating the detection process in optical SNSPD to include the effects of an applied magnetic field. One of the most important predictions of our model is a dependence of the threshold current (the applied current that results in nearly 100% detection probability) on the absorption site of the photon [4]. A photon absorbed in the center of the superconducting strip requires a higher threshold current than a photon of the same energy absorbed close to the edge. Furthermore, we expect a linear relation between the photon energy and the threshold current that holds for each absorption site.

The magnitude of the slope increases from the center to the edge of the strip. Extrapolated to zero photon energy, the linear relations intersect at roughly the vortex-entry current, which defines the current at which vortices can enter the superconducting strip without photon absorption and without thermal excitation. This model has been successfully used to interpret experimental results that confirmed the position-dependent threshold current [5]. The application of an external magnetic field induces Meissner screening currents. The resulting magnetic field inside the superconductor can be calculated with the help of the London equation $\Delta H = H\lambda^2$, where λ is the magnetic penetration depth. The magnetic field is applied perpendicular to the strip in the z-direction $\vec{H} = (0, 0, H)$. For strip width and thickness below λ the field in the undisturbed equilibrium situation is found to be proportional to $\cosh\left(\frac{x}{\lambda}\right)$ and the current density varies linearly across the strip. The non-equilibrium situation after the absorption of a photon results in a diffusive cloud of excess quasi-particles and as a consequence in a time- and position-dependent magnetic penetration depth λ. Using the density of excess quasi-particles and relating that to a change in λ, we were able to compute $H(r, t)$ for a series of times after the absorption of a photon at different positions across the strip.

The most interesting result from these simulations is an increased photon detection at the edges compared to the center of the strip. The linear relations between photon energy and threshold current change in response to the magnetic field in a way that the magnitude of the slope decreases in the center, but becomes even larger in a narrow area about 15 nm wide near the edge. This is visualized in Fig. 13.1 that shows the slope of the linear relation for selected photon positions as a function of the applied magnetic field. This particular simulation was done for a 150 nm wide strip, i.e. a position $x = 0$ indicates a photon absorbed in the center, and x=70 stands for a photon absorbed 5 nm from the edge.

[1] K. Inderbitzin *et al.*,
Appl. Phys. Lett. **101**, 162601 (2015).

[2] M. Hotz, Bachelor thesis, University of Zurich (2015).

[3] G. Meili, Bachelor thesis, University of Zurich (2015).

[4] A. Engel *et al.*,
IEEE Trans. Appl. Supercond., **25(3)**, 2200407 (2015).

[5] J. J. Renema *et al.*,
Nano Letters, **15(7)**, 4541-4545 (2015).

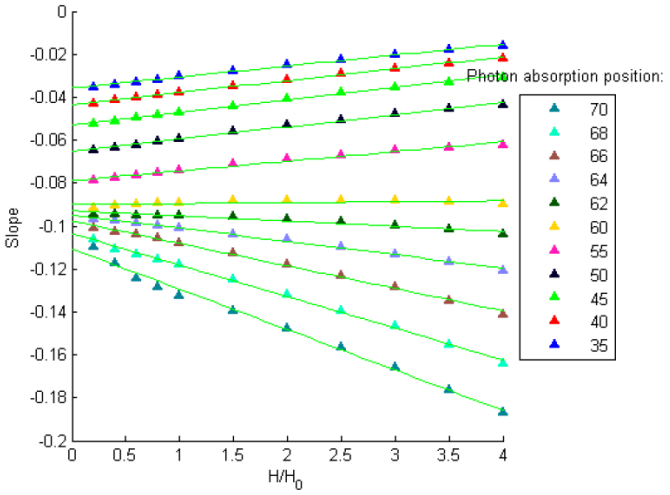

FIG. 13.1 – Slope of the linear relation between the threshold current and photon energy as a function of the applied magnetic field and photon absorption position.

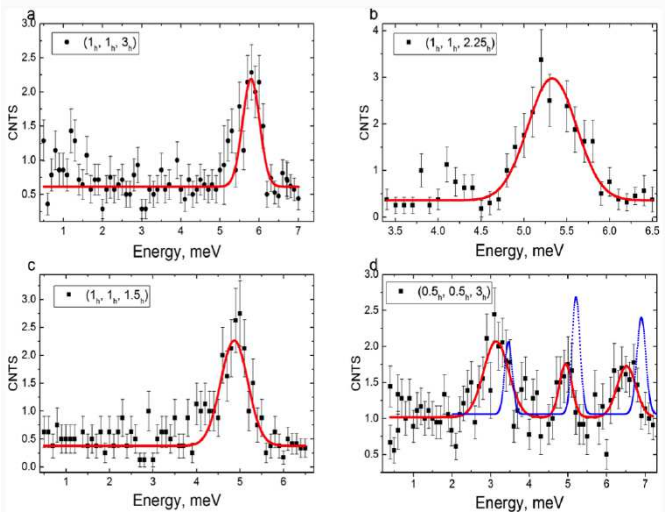

FIG. 13.2 – Energy scan of several neutron scattering Bragg peaks of $Ba_{0.1}Sr_{2.9}Cr_2O_8$ in comparison to $Sr_3Cr_2O_8$ (blue curve). The peaks are shifted towards lower energies as compared to pure $Sr_3Cr_2O_8$.

13.2 Experiments with $Ba_{3-x}Sr_xCr_2O_8$

The purpose of our experiments with $Ba_{3-x}Sr_xCr_2O_8$ has been twofold, both aimed at examining changes of the Jahn-Teller effect in the system and at inducing changes to the high-field phase transition of the spin system.

13.2.1 Manipulating the spin system

As described in previous annual reports, we have mainly examined polycrystalline samples of $Ba_{3-x}Sr_xCr_2O_8$. Such samples are well suited for macroscopic techniques such as magnetization experiments. However, coherence based techniques such as inelastic neutron scattering that allow a more direct examination of the magnetic interactions in the system require large and high quality single crystals. A next step was thus the preparation of single crystals based on a mirror furnace floating zone technique. This work has been carried out by our PhD student Alsu Gazizulina at the *Helmholtz-Institut für Materialien und Energie* in Berlin (HZB) in collaboration with the group of Prof. Bella Lake. We have successfully synthesized single-crystalline samples of $Ba_{3-x}Sr_xCr_2O_8$ with $x \in \{2.9,\ 2.8\}$.

To assess the anticipated changes of the magnetic spin interactions, we have carried out inelastic neutron scattering experiments on $Ba_{0.1}Sr_{2.9}Cr_2O_8$. From the preliminary results, we can conclude that the intra-dimer interaction constant J_0 indeed decreases with decreasing Sr content x (see Fig. 13.2). This is in accordance with our corresponding magnetization experiments [6].

These experiments will be extended to examine additional Bragg reflections for $Ba_{0.1}Sr_{2.9}Cr_2O_8$, allowing us to correctly estimate the changes of all relevant interaction constants and greatly decreasing the corresponding experimental uncertainty.

13.2.2 Examining the Jahn-Teller effect

As we have already established that the strength of the Jahn-Teller distortion in $Ba_{3-x}Sr_xCr_2O_8$ depends on the Sr content x, our current experiments aim at estimating the transition temperature T_{JT} as a function of x and examining the implications for the electronic interactions aside from the magnetic interaction constants.

The crystal structure has been investigated using neutron powder diffraction experiments on $Ba_{0.2}Sr_{2.8}Cr_2O_8$ and $Ba_{0.8}Sr_{2.2}Cr_2O_8$ for temperatures between 2 K and 300 K. We have observed the scattering intensity of Bragg peaks that are suppressed in the highly symmetric room temperature phase, but gradually gain in intensity due to the structural distortion upon cooling the crystal system.

From these experiments, we found that T_{JT} is decreasing strongly for decreasing x. However, as we used powder samples, the uncertainty of about 20 K is rather large, and the number of different stoichiometries is too small to make more general statements. To address this issue, we have performed additional heat capacity experiments, where the Jahn-Teller distortion can be identified by a fea-

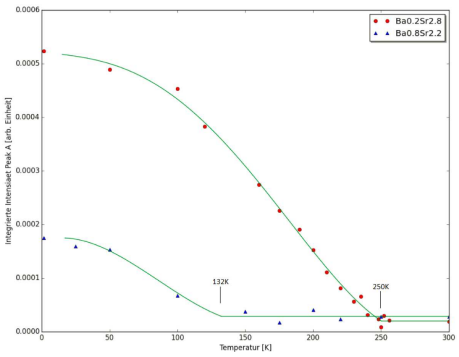

FIG. 13.3 – Integrated neutron powder diffraction intensity of Bragg peaks that are suppressed in the symmetric high temperature phase of $Ba_{3-x}Sr_xCr_2O_8$.

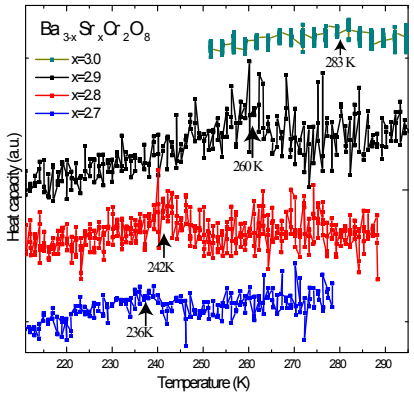

FIG. 13.4 – Heat capacity traces for $Ba_{3-x}Sr_xCr_2O_8$. The arrows mark the Jahn-Teller transitions.

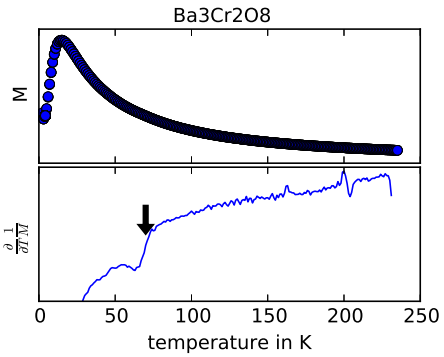

FIG. 13.5 – Magnetization M and temperature derivative $\frac{\partial}{\partial T}\frac{1}{M}$ of the inverse magnetization of $Ba_3Cr_2O_8$ as a function of the temperature. The arrow marks the Jahn-Teller transition.

ture in the heat capacity versus temperature. These experiments, performed for $x \in \{3.0,\ 2.9,\ 2.8,\ 2.7\}$, confirm the decrease of T_{JT} with decreasing x (see Fig. 13.4).

We have very recently established that the Jahn-Teller transition temperature can also be obtained by carefully analyzing the magnetization of $Ba_3Cr_2O_8$ as a function of the temperature (see Fig. 13.5). Here, the transition temperature can be obtained as a feature of the first temperature derivative $\frac{\partial}{\partial T}\frac{1}{M(T)}$ of the inverse magnetic moment $M(T)$. These experiments are currently being expanded to the full solid solution series $Ba_{3-x}Sr_xCr_2O_8$.

[6] H. Grundmann *et al.*,
New Journal of Physics, **18**, 033001 (2016).

13.3 Metamagnetism in $CsCo_2Se_2$

Antiferromagnetically ordered (AFM) compounds that can undergo a phase transition to a ferromagnetically ordered (FM) state upon the application of an external magnetic field are referred to as metamagnets [7]. If an external magnetic field is large enough, the magnetic moments of all unbound electrons will eventually line up with the applied magnetic field, causing a large overall magnetic moment [8]. Commonly, very large magnetic fields are necessary in order to observe so-called spin-flip or spin-flop metamagnetic transitions of compounds with an AFM ground-state.

Among the compounds ACo_2X_2 (with A = K, Rb, Cs, Tl and X = S, Se), which are related to the iron-based superconductors, $CsCo_2Se_2$ and $TlCo_2Se_2$ are the only two antiferromagnets [9, 10]. The other compounds have been found to order ferromagnetically at temperatures between $T_C \approx 50$ K and 110 K [9, 10]. In $TlCo_2Se_2$ the magnetic moments were found to order in a non-collinear incommensurate magnetic structure leading to an overall zero net magnetic moment [11, 12]. This phase has received considerable experimental and theoretical attention, because it is one of the few cobalt-based compounds with non-collinear magnetic ordering (see, e.g., reference [13, 14]). We investigated the magnetic properties of the highly air-sensitive compound $CsCo_2Se_2$ [15], which we find to be an A-type antiferromagnet displaying a metamagnetic field-induced transitions initiated in external magnetic fields even below $\mu_0 H < 1$ T [16].

The magnetic structure of the ground state of $CsCo_2Se_2$ was investigated by a series of neutron powder diffraction (NPD) experiments. In Fig. 13.6a, we show the NPD data of pulverized $CsCo_2Se_2$ crystals at 100 K, which was collected with a wavelength of $\lambda = 1.886$ Å. Most reflections of the diffraction pattern can be well explained with a $ThCr_2Si_2$ structure type model with space group $I4/mmm$. The cell parameters are $a \approx 3.842$ Å and $c \approx 15.041$ Å at 100 K. Several additionally observed Bragg reflections cannot be explained solely with this structure model, or with known phases of the Cs-Co-Se phase diagram. They can most likely be attributed to a decomposition product of the extremely air-sensitive $CsCo_2Se_2$ compound. A similar sensitivity to moisture and air has earlier been observed for the chemically closely related $A_{1-x}Fe_{2-y}Se_2$ phases [17, 18].

At the bottom of Fig. 13.6, we show the NPD data of the same polycrystalline $CsCo_2Se_2$ sample at 1.5 K collected with a wavelength of $\lambda = 1.886$ Å. We observe a single magnetic diffraction peak at $2\Theta = 7.2°$ that corresponds to the (001) reflection of the tetragonal crystal structure on hand. It can be indexed with the propagation vector $\vec{k} = [1, 0, 0]$. This implies an AFM order for the body centered Bravais lattice. We can explain our data if the magnetic moments form FM sheets with the spin direction in the *ab* plane with a magnetic coupling of $0.20(1)\mu_{\mathrm{Bohr}}$/Co. The corresponding real-space magnetic structure is depicted in Fig. 13.7. This magnetic structure it commonly referred to as A-type antiferromagnetism.

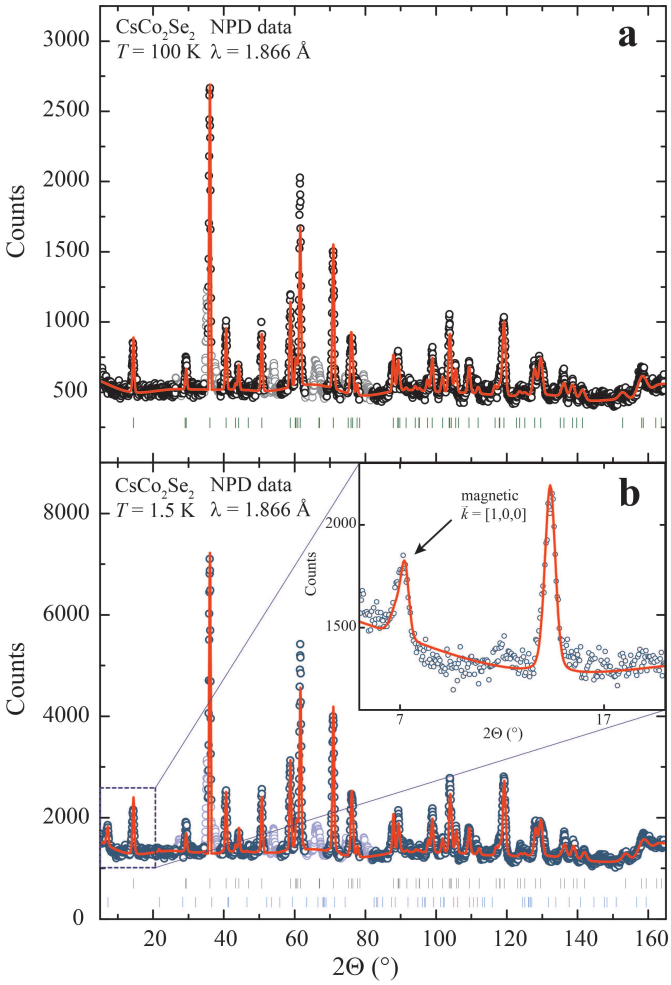

FIG. 13.6 – Neutron powder diffraction pattern of polycrystalline $CsCo_2Se_2$ at 100 K (a) and 1.5 K (b) collected with a wavelength of $\lambda = 1.886$ Å. Black and blue circles: observed patterns; red curves: calculated patterns; black tic marks: calculated peak positions for the crystal structure of $CsCo_2Se_2$; blue tic marks: calculated peak positions for the magnetic reflections of $CsCo_2Se_2$.

FIG. 13.7 – Crystal and magnetic structure of $CsCo_2Se_2$, the magnetic moments on the cobalt position of the A-type AFM structure are displayed as red arrows.

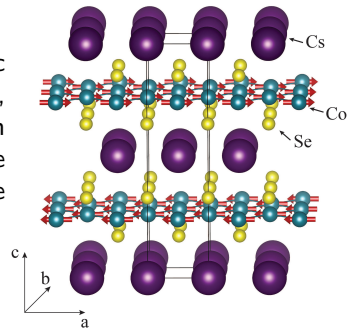

In Fig. 13.8, we show the magnetic susceptibility as $\chi = M/H$ (a) and the magnetization (b) in a temperature range between $T = 5$ K to 100 K with the external field $\mu_0 H$ perpendicular to the c axis of $CsCo_2Se_2$. The clearly pronounced metamagnetic transition from a AFM orientation to a FM orientation of the magnetic moments can be observed in these measurements. The transition temperature is shifted only slightly to lower temperatures with higher magnetic fields. A clear saturation of the magnetic moments in a FM or canted AFM alignment is found in fields greater than $\mu_0 H \approx 6$ T, while the transition is observed to be continuous. As expected, the field dependence of the magnetization $M(H)$ of $CsCo_2Se_2$ deviates from a common AFM behaviour and further supports the scenario of a spin reorientation and therefore of a metamagnetic transition (not shown here).

Four different magnetic phases can be identified in $CsCo_2Se_2$: a paramagnetic high-temperature phase (PM), an antiferromagnetically ordered phase (AFM), one or more metamagnetic phase transitions (MM), and a ferromagnetically ordered phase (FM) (see Fig. 13.9). This nomenclature is chosen on the basis of earlier reports of similar magnetic properties. It should be noted that all of the observed transitions are continuous and that all here determined critical fields are not strict quantities.

FIG. 13.8 – Magnetic susceptibility χ (a) and the magnetization m (b) in a temperature range of $T = 5$ K to 100 K in magnetic fields $\mu_0 H$ from 1 T to 7 T in 0.5 T steps.

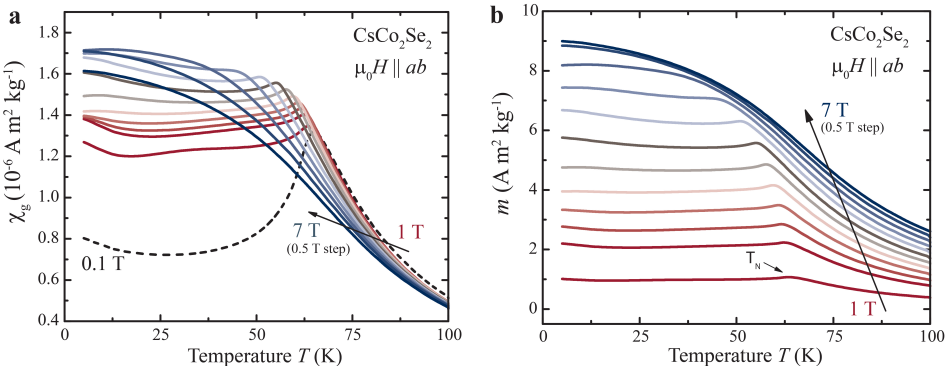

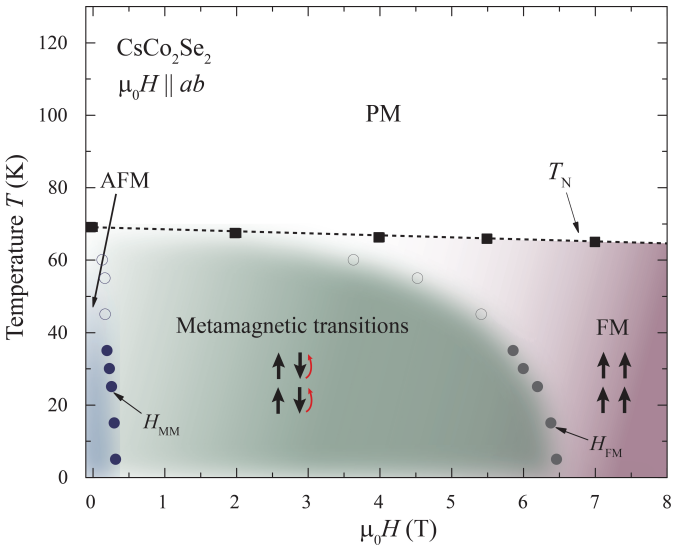

FIG. 13.9 – Phase diagram of $CsCo_2Se_2$ for magnetic fields up to 7 T, determined from field dependent magnetization measurements.

Furthermore, at higher temperatures the transitions broaden and are less pronounced in the field-dependent magnetization $M(H)$ (represented in Fig. 13.9 by open circles). The observed phase diagram is in qualitative agreement with other metamagnetic materials. Layered A-type antiferromagnetic materials often undergo metamagnetic transitions in external magnetic fields parallel to the antiferromagnetically ordered spin lattices, because the interlayer AFM coupling is in such an alignment comparably weak.

Our study [15] characterizes $CsCo_2Se_2$, which is chemically and electronically posed closely to the $A_xFe_{2-y}Se_2$ superconductors, as a host of versatile magnetic interactions that likely can be tuned by chemical variation of the interlayer distance. In further studies, the strong correlation between the structure and magnetism in these materials may give new insights into the nature of the magnetic and superconducting interactions in the $ThCr_2Si_2$-related superconductors and magnets.

[7] E. Stryjewski and N. Giordano, 1977 *Advances in Physics* **26** 487.

[8] E.P. Wohlfarth and P. Rhodes P, 1962 *Philosophical Magazine* **7** 1817.

[9] G. Huan G and M. Greenblatt, 1989 *J. Less-Common Met.* **156** 247.

[10] J. Yang, B. Chen, H. Wang, Q. Mao, M. Imai, K. Yoshimura, and M. Fang, 2013 *Phys. Rev. B* **88** 064406.

[11] R. Berger, M. Fritzsche, A. Broddefalk, P. Nordblad, and B. Malaman, 2002 *J. Alloys Compd.* **343** 186.

[12] R. Lizarraga, S. Ronneteg, R. Berger, A. Bergman, O. Eriksson, and L. Nordström, 2004 *Phys. Rev. B* **70** 024407.

[13] H. K. Jeong, T. Valla, R. Berger, P. D. Johnson, and K. E. Smith, 2007 *EPL* **77** 27001.

[14] S. Ronneteg, S. Felton, R. Berger, and P. Nordblad, 2003 *J. Magn. Magn. Mater.* **299**, 53.

[15] F. von Rohr *et al.*, accepted in *J. Phys: Condensed Matter.*

[16] F. von Rohr, A. Krzton-Maziopa, V. Pomjakushin, H. Grundmann, Z. Guguchia, W. Schnick, A. Schilling, http://arxiv.org/abs/1605.01113.

[17] S. Weyeneth, M. Bendele, F. von Rohr, P. Dluzewski, R. Puzniak, A. Krzton-Maziopa, S. Bosma, Z. Guguchia, R. Khasanov, Z. Shermadini, A. Amato, E. Pomjakushina, K. Conder, A. Schilling, and H. Keller, 2012 *Phys. Rev. B* **86** 134530.

[18] V. Y. Pomjakushin, E. V. Pomjakushina, A. Krzton-Maziopa, K. Conder and Z. Shermadini, 2011 *J. Phys.: Condens. Matter* **23** 156003.